OPEN ACCESS

Original research

Characteristic immune cell interactions in livers of children with acute hepatitis revealed by spatial single-cell analysis identify a possible postacute sequel of COVID-19

Felix Röttele,[1] Andreas Zollner ,[2] Carolin Mogler,[3] Muhammed Yuksel,[4] Cigdem Arikan,[4] Vivien Karl,[1] Judith Helene Aberle,[5] Stephan W Aberle,[5] Hubert Kogler,[6] Andreas Vécsei,[6] Julia Vodopiutz,[7] Henrike Salié ,[1] Anne Gräser,[1] Laurenz Krimmel ,[1] Pius Martin,[1] Eberhard Lurz,[8] Felix Immanuel Maier,[9] Lena Woelfle,[10] Susana Nobre,[11] Isabel Goncalves,[11] Lisa Kern,[12] Martin Schwemmle,[12] Tobias Boettler ,[1] Maike Hofmann ,[1] Peter Hasselblatt ,[1] Robert Thimme ,[1] Herbert Tilg ,[2] Thomas Müller ,[13] Georg Friedrich Vogel ,[13,14] Bertram Bengsch [1,15]

► Additional supplemental material is published online only. To view, please visit the journal online (https://doi.org/10.1136/gutjnl-2024-333880).

For numbered affiliations see end of article.

Correspondence to
Professor Bertram Bengsch; bertram.bengsch@uniklinik-freiburg.de and Dr Georg Friedrich Vogel; georg.vogel@i-med.ac.at

FR, AZ and CM are joint first authors.
GFV and BB are joint senior authors.

Received 12 September 2024
Accepted 24 November 2024
Published Online First
5 April 2025

Check for updates

© Author(s) (or their employer(s)) 2025. Re-use permitted under CC BY-NC. No commercial re-use. See rights and permissions. Published by BMJ Group.

To cite: Röttele F, Zollner A, Mogler C, *et al*. *Gut* 2025;**74**:1486–1499.

ABSTRACT

Background A rise in paediatric cases of acute hepatitis of unknown origin (AHUO) was observed in 2022, some requiring liver transplantation. A link to adeno-associated virus 2 infection and CD4$^+$T-cell mediated disease was reported in cohorts in the UK and USA but does not explain all cases.

Objective To determine the intrahepatic immune cell interactions in the inflamed liver and a possible contribution of SARS-CoV-2 infection.

Design Patients with acute non-A non-E hepatitis (10/12 AHUO, 2/12 subacute) during February 2022–December 2022 undergoing liver biopsy were recruited in a European patient cohort. Hepatological, virological, histopathological and highly multiplexed spatial and single-cell analyses of liver biopsies were performed.

Results Patients were negative for adenoviral and SARS-CoV-2 PCR. Three patients had a positive adenoviral serology and 10/12 patients had a history or serological evidence of SARS-CoV-2 infection. Imaging mass cytometry identified significant intrahepatic immune infiltration with an enrichment of CD8$^+$T-cells. The highest CD8 infiltration and concomitant peripheral immune activation were observed in patients with the most severe hepatitis. CD8$^+$T-cell infiltration was connected to histomorphological interface hepatitis and bridging necrosis. Cellular neighbourhood analysis indicated disease-associated microanatomic interactions between CX3CR1$^+$ endothelial and myeloid cell populations, interacting with effector CD8$^+$T-cells suggesting a pathogenic cellular triad. Of note, we detected intrahepatic SARS-CoV-2 antigens in ACE2-expressing cells in the areas with significant pathology in 11/12 samples using several different detection methods.

WHAT IS ALREADY KNOWN ON THIS TOPIC

⇒ After the release of lockdown measures during the COVID-19 pandemic, a surge of cases of acute hepatitis cases of unknown origin (AHUO) among children was identified particularly in the UK and connected to a possible epidemic event by adenoviral/adeno-associated virus 2 infection with a role for CD4 T-cells. However, this association was not observed in several other cohorts suggesting other potential causative agents. Small case series reported paediatric cases of AHUO after an acute COVID-19 infection; however, immunological, virological and histopathological evidence is lacking.

WHAT THIS STUDY ADDS

⇒ This study performed an in-depth characterisation of the cellular microenvironment in the inflamed livers of paediatric AHUO patients using highly multiplexed imaging combined with the detection of viral antigens. It identifies characteristic pathogenic cellular interactions between effector CD8 T cells, myeloid cells and endothelial cells in areas with the presence of SARS-CoV-2 antigens connected to more severe hepatitis. The clinical and virological workup indicates these cases of AHUO could reflect postacute sequelae of COVID-19 (PASC) and suggest steroid therapy as a possible management strategy.

Gut: first published as 10.1136/gutjnl-2024-333880 on 5 April 2025. Downloaded from http://gut.bmj.com/ on August 18, 2025 at Koc Universitesi. Protected by copyright, including for uses related to text and data mining, AI training, and similar technologies.

HOW THIS STUDY MIGHT AFFECT RESEARCH, PRACTICE OR POLICY

⇒ SARS-CoV-2 infection needs to be considered as a potential trigger of paediatric AHUO and testing for intrahepatic SARS-CoV-2 antigens should be considered. The persistence of viral proteins suggests residual viral niches after acute COVID-19 infection as a potential driver of the hepatic inflammation. Further studies are required to determine the optimal clinical management for PASC-hepatitis.

10/12 patients were treated with corticosteroid therapy and no liver transplantation was required.

Conclusions We identified a possible manifestation of an immune-mediated postacute sequel to COVID-19 associated with a characteristic immune infiltrate in children with AHUO. COVID-19 testing should be considered in paediatric AHUO.

INTRODUCTION

In early 2022, a strong increase in cases of acute hepatitis of unknown origin (AHUO) among children was noted, particularly in the UK.[1–8] The WHO definition of AHUO refers to a person presenting with acute non-A non-E hepatitis (NAEH) with serum transaminase levels >500 U/L, who is 16 years and younger, since 1 October 2021. In the diagnostic workup, a majority of UK cases were connected to positive tests for adenoviral infection in serum, stool or pharynx in some cases, with adenovirus 41F detected when subtyped.[1] Two studies from cohorts in the UK reported the identification of adeno-associated virus 2 (AAV2) in serum and liver samples in the majority of patients.[9–11] In that cohort, AAV2 infection was most likely acquired as a coinfection with human adenovirus that is usually required as a 'helper virus' to support AAV2 replication and connected to an MHC class II risk allele and CD4 T-cell responses.[11] Signatures of AAV2 immunity were also identified in some US AHUO cohorts.[12 13] Consecutively, the antiviral cidofovir has been used as a therapeutic option in some cases.[14] The association with adeno-associated or adeno-associated viridae was also observed—admittedly at different rates—in a historic paediatric acute liver failure (PALF) cohort.[9] Interestingly, other studies from Germany[15] and the USA[16] did not observe a similar viral association. Overall, during a similar time period, clinical presentation, aetiology and disease progression to PALF seem to differ among cohorts.[17]

NAEH is an established disease entity in children characterised by acute onset of hepatitis, with a varying degree of patients progressing to PALF eventually requiring liver transplantation (LT). NAEH is, therefore, also referred to as indeterminate PALF. While the definition of NAEH includes primarily the exclusion of viral hepatitis A–E, other possible underlying causes of acute hepatitis such as environmental exposures, drug toxins or metabolic or genetic disorders are tested for and are subsequently excluded. Presumably, NAEH comprises a spectrum of hepatitis with various, yet unclear, aetiologies, that might share common clinical, immunological and histological features. Other (non-A–E) viral infections are occasionally detected but the diagnostic workup frequently remains negative.[15] NAEH may also associate with hepatitis-associated aplastic anaemia (HAAA) eventually necessitating haematopoietic stem cell transplantation.[18–20] The histopathology of HAAA is characterised by intralobular CD8-positive T-cell infiltration.[21] Immunosuppressive therapy with corticosteroids and or antithymocyte globulin was shown to have some benefit for NAEH and HAAA[22] supporting the hypothesis of a T-cell-mediated autoimmunity.

In 2022, the rise in AHUO/NAEH incidence coincided with a reduction of hygiene precautions due to the global COVID-19 pandemic, which continued to top infection rates within the global population at the same time, particularly in children.[23] Hepatotropism of SARS-CoV-2 with or without acute hepatitis is well established.[24] COVID-19 can elicit significant immune-mediated pathology in many organs that involves many arms of the immune system but is frequently dominated by myeloid-T-cell interactions.[25] However, despite the established potential of direct SARS-CoV-2 infection of hepatocytes,[20] severe hepatic inflammation is rare. In addition, COVID-19-directed immunity elicited after vaccination may also cause liver damage, as suggested by cases of COVID-19-vaccine-induced liver injury in which highly activated $CD8^+$T-cells, including T-cells with SARS-CoV-2-specificity, were identified in the liver.[26 27] However, in the UK cohort, no AHUO patient was reported to have a history of COVID-19 vaccination.[10]

In the wake of the pandemic, it has become clear that SARS-CoV-2 infection can lead to many postacute sequelae in different organ systems. The highest risk for gastrointestinal manifestations was observed in the first 90 days after resolution of infection; however, data regarding postacute liver disease remain scarce.[28] Currently, it remains unclear if COVID-19 may cause AHUO. In an early study including five paediatric cases of NAEH, among which two patients required LT, the authors noted that a COVID-19 infection preceded disease onset and no other cause was identified.[3] In the analysis of the paediatric cohorts that were associated with adenoviral infection, SARS-CoV-2-positive PCR indicating active infection was observed in 8.9%–12.8% of cases[8 10] but up to 52% of patients tested positive for SARS-CoV-2-nucleocapsid IgG.[11] Overall, these data indicate the potential for immune-mediated COVID-19-associated liver injury.

We, therefore, set out to understand if the NAEH cases observed in our multicentre paediatric cohort (collected during a comparable timeframe during the pandemic) reflected a distinct immunopathological landscape and tested for a possible association with prior adenoviral or COVID-19 infection. The highly multiplexed spatial single-cell analysis of the livers of paediatric patients performed in this work allowed the in-depth immunophenotypic characterisation of hepatic inflammatory infiltrates and pointed to a pathology dominated by $CD8^+$T-cell-myeloid-endothelial cell interactions. Intrahepatically, SARS-CoV-2 antigens were detected in association with ACE2 expression in the immune-infiltrated areas. These data suggest COVID-19 as a possible driver of AHUO/NAEH, fitting to a manifestation of a hepatic postacute sequel of COVID-19 (PASC). Despite the presentation of severe liver inflammation, no patient subsequently required LT, possibly due to immunosuppressive corticosteroid therapy.

RESULTS

Study cohort

12 paediatric patients presenting with AHUO undergoing liver biopsy were recruited to the study in 2022 in centres in Austria, Germany, Portugal and Turkey. 10 met the WHO-inclusion criteria for AHUO/acute NAEH, whereas 2 patients had elevated transaminases >10×upper limit of normal (ULN) but below the cut-off of 500 U/L and were therefore termed 'subacute' (table 1). The median age was

Gut: first published as 10.1136/gutjnl-2024-333880 on 5 April 2025. Downloaded from http://gut.bmj.com/ on August 18, 2025 at Koc Universitesi. Protected by copyright, including for uses related to text and data mining, AI training, and similar technologies.

Table 1 Cohort and clinical parameters

Patient	1	2	3	4	5	6	7	8	9	10	11	12
Sex	Female	Male	Female	Female	Female	Male	Male	Female	Female	Female	Male	Female
Age (months)	118	39	114	84	32	20	168	184	168	156	84	127
WHO criteria	Acute	Acute	Acute	Acute	Acute	Acute	Acute	Acute	Acute	Subacute	Subacute	Acute
Symptoms												
Jaundice	Yes	No	Yes	No	Yes	Yes	Yes	Yes	Yes	No	No	Yes
Fever	No	No	No	Yes	Yes	Yes	No	Yes	Yes	Yes	Yes	No
Diarrhoea	No	Yes	No	No	Yes	Yes	No	Yes	Yes	Yes	Yes	No
Vomiting	No	No	Yes	Yes	No	No	Yes	Yes	Yes	Yes	Yes	No
Abdominal pain	Yes	Yes	No	Yes	No	No	No	No	No	No	No	No
Liver tests												
Total bilirubin (µmol/L):	367.2	3.4	138.51	16	256.7	208.6	449.7	4.1	5.13	144	3.93	75.5
ALT (U/L)	2535	890	2516	1124	1901	1068	1800	714	1100	488	402	611
AST (U/L)	2465	677	1458	871	2372	991	2246	530	860	427	378	247
GGT (U/L):	347	34	151	98	189	77	41	378	340	142	27	501
LDH (U/L):	553	411	439	577	484	384	578	187	580	173	431	285
INR	1.6	0.98	1.07	NA	2.6	1.81	2.2	1.13	2.8	1	1.1	NA
ISHAK-Score	4	2	9	4	9	6	1	7	1	3	5	3
Viral tests												
Adenovirus Serology	Negative	Negative	NA	Negative	IgG positive (stool)	Negative	IgM, IgG positive	NA	NA	NA	NA	IgG positive
Adenoviurs PCR (Serum)	Negative	Negative	Negative	Negative	Negative	Negative	Negative	Negative	Negative	Negative	Negative	Negative
Adenoviurs PCR (liver)	Negative	Negative	Negative	NA	NA	NA	NA	NA	NA	NA	NA	NA
Adeno-associated-virus 2 PCR (liver)	Negative	Negative	Negative	NA	NA	NA	NA	NA	NA	NA	NA	NA
Epstein-Barr-Virus (Serology)	Negative	Negative	Negative	Negative	Negative	Negative	Negative	Negative	Negative	Negative	Negative	Negative
SARS-CoV-2												
PCR (swab)	Negative	Negative	Negative	Negative	Negative	Negative	Negative	Negative	Negative	Negative	Negative	Negative
PCR (liver)	Negative	Negative	Negative	NA	NA	NA	NA	NA	NA	NA	NA	NA
RNAscope (liver)	NA	NA	NA	Negative	Negative	NA	NA	Negative	Negative	Negative	Negative	Negative
Known infection (months prior):	2	3	3	NA	NA	NA	No	2	1	1	1	2.5
Spike serology (U/L)	NA	Positive	NA	Positive	Positive	Negative	Negative	>250	>100	152	183	NA
Nucleocapsid serology	Positive	Negative	Positive	Positive	Negative	Negative	Negative	Negative	Negative	Negative	Negative	NA
Vaccinated	No	No	No	No	No	No	No	Yes	Yes	Yes	Yes	No
Others	Negative	Negative	Rhino/Entero (nasal)	Rota positive	HHV6, Rota (stool), Sapo (stool) positive	Negative	Negative	Negative	Negative	Negative	Negative	Negative
Toxicologic workup	Negative	Negative	Negative	Negative	Negative	Negative	Negative	Negative	Negative	Negative	Negative	Negative
Autoantibodies	Negative	Negative	ANA–, SMA–	LKM1+	LKM+	Negative	GP210–	ANA+, AMA+, SMA+	Negative	ANA+, SMA+	SMA+, ANA+	LKM1+
Therapy												
Steroids	Yes	Yes	Yes	Yes	Yes	No	Yes	Yes	Yes	NA	Yes	Yes

Continued

Gut: first published as 10.1136/gutjnl-2024-333880 on 5 April 2025. Downloaded from http://gut.bmj.com/ on August 18, 2025 at Koc Universitesi. Protected by copyright, including for uses related to text and data mining, AI training, and similar technologies.

Table 1 Continued

Patient	1	2	3	4	5	6	7	8	9	10	11	12
Follow-up	Improved	Improved	Improved	Improved	Improved	Improved	Improved	Improved	Improved	NA	Improved	Improved
Onset steroids to AST/ALT improvement	Days	Days	Days	Weeks	Days	NA	Weeks	Weeks	Weeks	NA	Weeks	
LT	No	No	No	No	No	No	No	No	No	No	No	No
Relapse in follow-up	No	No	Yes	No	No	No	No	Yes	No	No	No	No

ALT, alanine-aminotransferase; AST, aspartate-aminotransferase; LDH, lactate dehydrogenase; LT, liver transplantation.

9.5 years at hospitalisation. Patients presented with typical symptoms of acute hepatitis and had elevated total bilirubin (median 141 µmol/L) and elevated alanine-aminotransferase (ALT) (median 1084 U/L), aspartate-aminotransferase (AST) (median 865 U/L) and lactate dehydrogenase (LDH) (median 461 U/L). Coagulation was slightly impaired (median INR 1.36) (table 1). Toxicologic workup was negative in all patients. In serum, all patients tested adenovirus PCR-negative. Autoantibodies for LKM1 and SMA were detected in 25% (3/12) of patients. Viral panel testing identified Rotavirus in stool in two patients (one reporting diarrhoea who was also positive for sapovirus (stool) and serum-positive for HHV6). History of SARS-CoV-2 infection was reported in 8/12 patients with a median of 2 months prior to presentation with AHUO. Vaccination for SARS-CoV-2 was reported in 33% of patients (4/12). All patients were tested by swab and were SARS-CoV-2-PCR negative at admission. During clinical admission, steroids were administered in 10/12 patients. AHUO improved in all patients in which follow-up was available. Two patients had hepatitis relapse after steroid weaning. LT was not required.

Histopathology

H&E stainings (online supplemental figure 1) were re-evaluated by an experienced liver pathologist blinded to the sample information (CM). All cases presented with a predominant hepatic pattern of liver injury. Portal inflammation was present in all cases, interface hepatitis in 10 cases (83%) and (confluent) necrosis in 10 cases (83%), resulting in a median ISHAK score of 5 (range 1–9). Mild portal fibrosis was present in two patients. Five patients (42%) presented with a prominent eosinophilic infiltrate in portal tracts. One case presented with cholestasis. Typical features of autoimmune hepatitis (AIH) (such as enriched plasma cell infiltrates or emperipolesis or ductular proliferations or bile duct lymphocytosis) were not observed. Histopathology was not typical for adenoviral or AAV2 infection, since the cases differed significantly from classical histology of adenoviral infection or liver AAV-associated-transplantation cases: There were no inclusion bodies, no significant bile duct injury was observed and only one patient experienced a focal ductular reaction.[9 29 30] Furthermore, we observed adenoviral-untypical hepatocellular ballooning and sinusoidal dilation. Classical signs of chronic liver damage were absent. In sum, histopathological evaluation was consistent with acute hepatitis, of possible viral origin.

Highly multiplexed imaging mass cytometry analysis of livers from children with AHUO reveals significant tissue pathology and immune cell infiltration

To understand the underlying tissue pathology and possible immunopathogenesis, we set out to perform a deep spatial profiling of the inflamed livers using highly multiplexed imaging mass cytometry (IMC). The 40-plex panel was designed to dissect the liver parenchymal cell populations, major adaptive and innate immune subsets as well as markers of immune activation and metabolic function at single-cell resolution (figure 1B and online supplemental table 1). For COVID-19-related analysis, antibodies staining for ACE2 and Spike protein were included, as established in prior studies.[25 26]

12 liver biopsies from AHUO patients (10 acute and 2 subacute) were available for IMC analysis. Control samples

Gut: first published as 10.1136/gutjnl-2024-333880 on 5 April 2025. Downloaded from http://gut.bmj.com/ on August 18, 2025 at Koc Universitesi. Protected by copyright, including for uses related to text and data mining, AI training, and similar technologies.

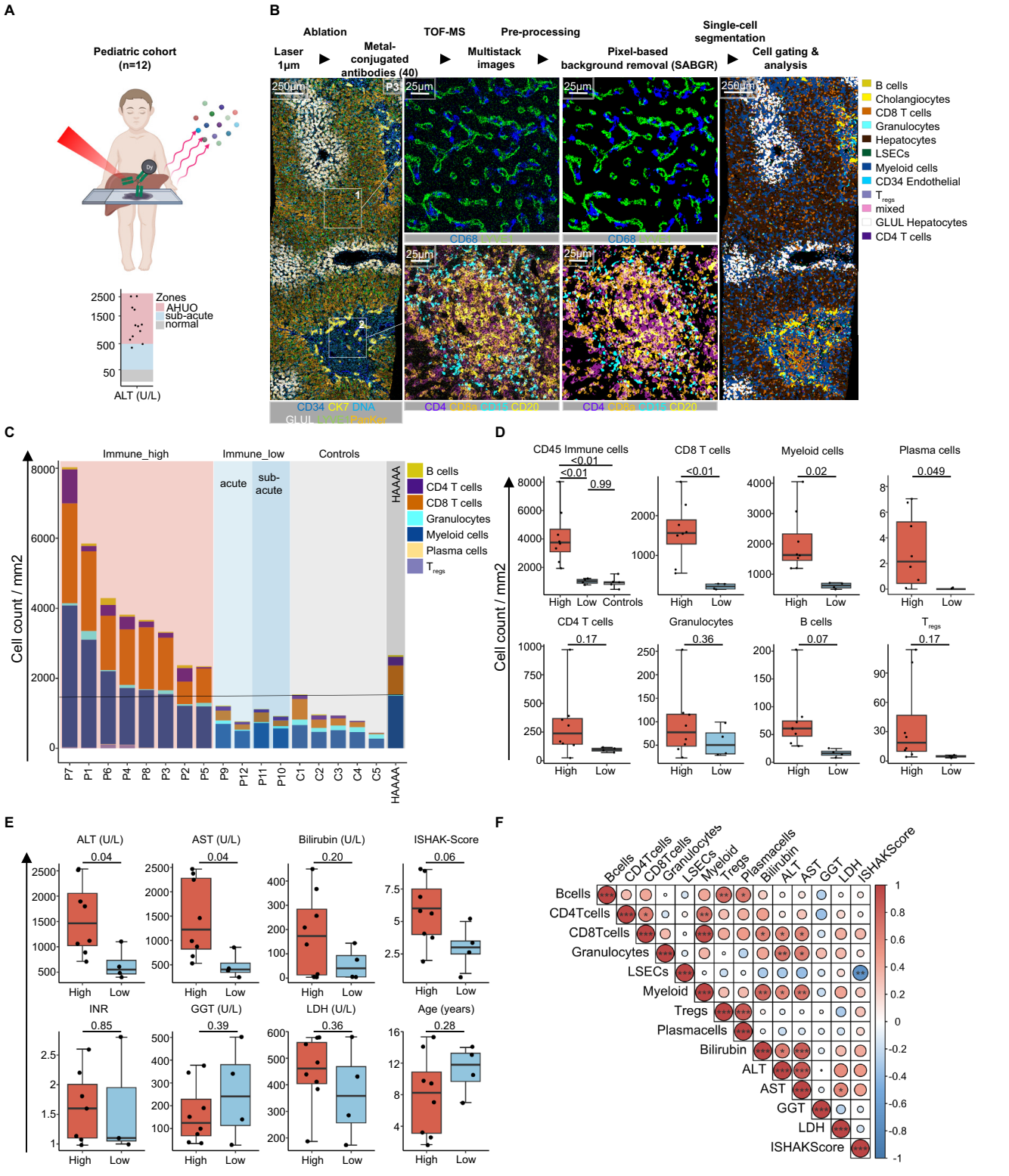


Figure 1 CD8+T-cell dominated immune cell infiltration correlates with severity of AHUO. (A) Cohort overview. ALT levels are indicated. Dotted line indicates WHO criteria/threshold for acute hepatitis (ALT>500 U/L). Created in BioRender. (B) Schematic depiction of IMC workflow and exemplary visualisation of parenchymal and immune cell types (P3) (scale bar=25 µm, otherwise depicted in picture). (C) Stacked bar chart of CD45+ immune cells abundances per mm2: CD20+B cells (yellow), CD3+CD8+ T-cells (orange), CD3+CD4+ T-cells (purple), CD15+ granulocytes (cyan) and CD68+ myeloid cells (blue), CD3+/CD4+/FoxP3+ Tregs (light purple), CD38+/CD20+ Plasma cells (light yellow) across paediatric cohort and controls. Dotted line divides groups: immune_high and immune_low. (D, E) Boxplots (median±SD) of immune cell subsets or clinical parameters, respectively. Immune_high, immune_low and control groups are indicated. (F) Spearman-correlation matrix of cell types and clinical parameters. Statistics: Kruskall-Wallis with Dunn's multiple comparison test for comparing immune_high versus immune_low versus controls (D), Mann-Whitney U test with for immune_high versus immune_low (D, E). P values indicated in boxplots. Spearman correlation (*p<0.05, **p<0.01, ***p<0.001) in (F). AHUO, acute hepatitis of unknown origin; ALT, alanine-aminotransferase; AST, aspartate-aminotransferase; IMC, imaging mass cytometry; LDH, lactate dehydrogenase.

Gut: first published as 10.1136/gutjnl-2024-333880 on 5 April 2025. Downloaded from http://gut.bmj.com/ on August 18, 2025 at Koc Universitesi. Protected by copyright, including for uses related to text and data mining, AI training, and similar technologies.

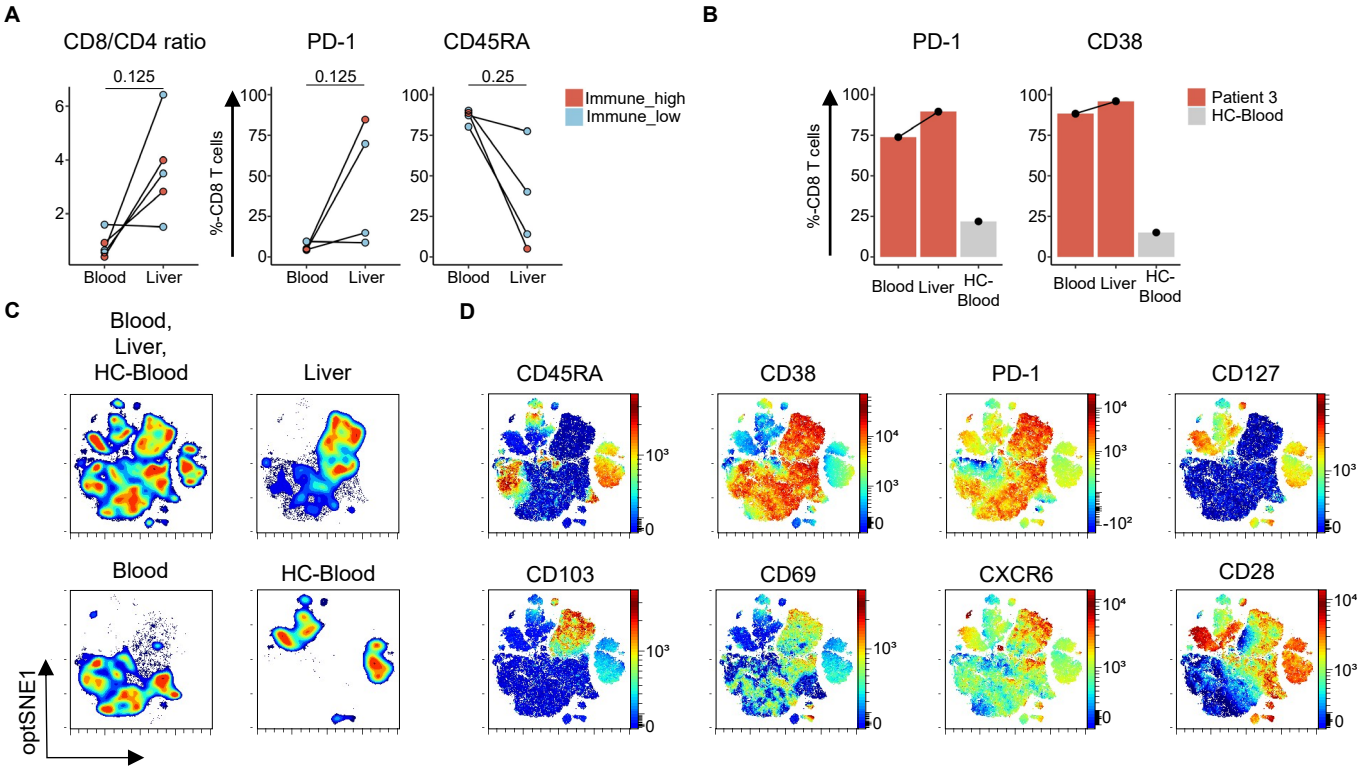


Figure 2 Flow cytometry indicates intrahepatic and peripheral CD8+T-cell activation. (A) Patients 3, 8–11 were analysed by flow cytometry. Scattered dot plots indicating the CD8/CD4 T-cell ratio, PD-1 and CD45RA expression in liver and blood (PBMCs) samples. (B, C) FACS analysis of patient 3. (B) Quantification of PD1 and CD38 expression in comparison to healthy control (HC-Blood). (C) tSNE markers is shown by heat colouring on the tSNE map. Statistics: Wilcoxon test (A). representation of CD8+T-cells between patient liver, blood and HC-Blood. (D) Expression of indicated T-cell. PBMCs, peripheral blood mononuclear cells; tSNE, t-distributed stochastic neighbor embedding.

included a case of prepandemic HAAA and five macroscopically healthy control liver tissues. Tissue sections were immunolabeled with antibodies coupled to metal isotopes and spatial expression data were obtained after laser ablation at 1 µm resolution by mass spectrometry analysis of metal labels. Bioinformatic processing included artificial intelligence (AI)-aided cell segmentation and semiautomated background removal (figure 1B). As illustrated in figure 1B, this approach allowed us to determine the hepatic microarchitecture at single-cell resolution and allowed the identification of parenchymal hepatocytes as well as Lyve1$^+$ liver sinusoidal endothelial cells (LSECs) and immune cell subtypes.

Single-cell analysis identifies CD8$^+$T-cell and myeloid cell infiltration connected to the severity of acute hepatitis

Quantification of immune cells revealed significant heterogeneity between patient samples. 8/12 patient samples showed higher immune cell infiltration than observed in controls (figure 1C). We accordingly categorised the patient cohort into immune cell-enriched (immune_high>1750 cells/mm^2) and immune_low (<1750 cells/mm^2) groups. Interestingly, in the immune_high group, we observed a significant enrichment of CD8$^+$T-cells, myeloid cells and plasma cells (figure 1D). Other immune cell populations such as CD4$^+$T-cells, Tregs, B cells and granulocytes only displayed non-significant trends to higher hepatic infiltration in the immune_high group. Interestingly, the immune infiltrate differed significantly from patients with AIH which exhibited high immune cell infiltration and had a significantly different composition of the immune cell infiltrate (online supplemental figure 2A,B).

We next explored the connection with clinical parameters. We identified significantly higher ALT and AST levels in immune_high patients while no significant differences in bilirubin, GGT, INR and LDH levels or age were observed (figure 1E). Correlation analysis revealed an association of CD8$^+$T-cells, granulocytes and myeloid cells with degree of liver inflammation, whereas LSEC density was conversely associated with low AST and Bilirubin levels and a low ISHAK score (figure 1F), suggesting a role for these cell populations in disease pathogenesis. Together, these analyses indicate a clear connection between the severity of liver disease and the degree of histologic immune cell infiltration.

The intrahepatic immune activation is reflected by CD8$^+$T-cell activation in the peripheral blood

We next asked whether the intrahepatic T-cell infiltration was connected to immunological changes in the peripheral blood. Paired peripheral and intrahepatic FACS analyses were performed in a subset of patients (Pts. 3, 8, 9, 10, 11). A higher CD8/CD4 ratio in the liver compared with the peripheral blood was observed in most patients analysed by FACS (4/5), with reduced CD45RA expression and higher PD-1 expression of CD8$^+$T-cells indicating infiltration of activated effector cells (figure 2A). High-parametric flow cytometry was performed for a patient from the Immune_high group. We found highly activated peripheral CD8$^+$T-cells, with high expression of CD38, PD-1 and CD69 and

Gut: first published as 10.1136/gutjnl-2024-333880 on 5 April 2025. Downloaded from http://gut.bmj.com/ on August 18, 2025 at Koc Universitesi. Protected by copyright, including for uses related to text and data mining, AI training, and similar technologies.

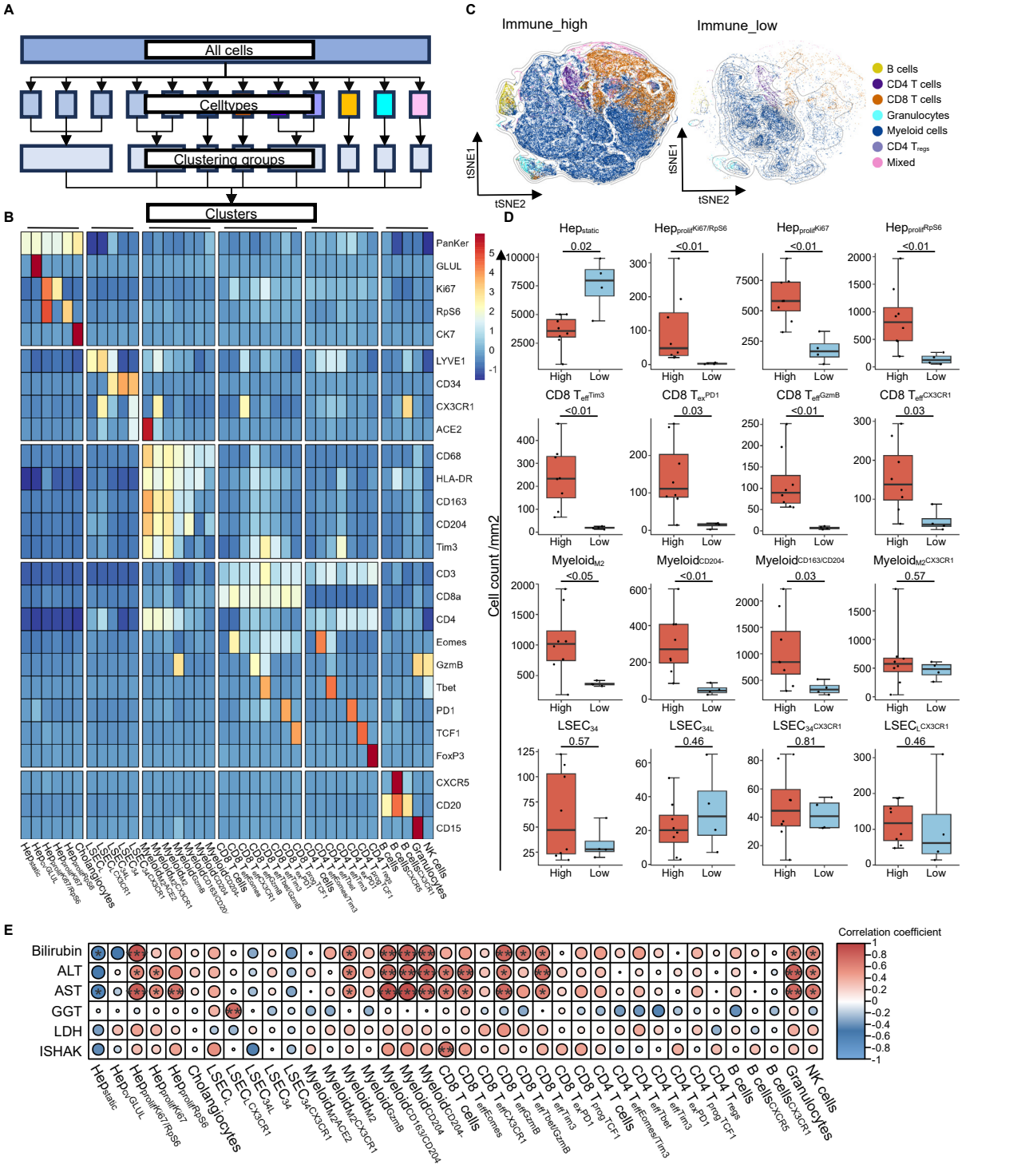


Figure 3 High-dimensional cluster analysis reveals disease-associated immune cell subsets. (A) Schematic of multilevel phenograph clustering approach, using gating-based random-forest guided prediction identification of cell types and meta clustering based on overlapping markers. (B) Z-scored Heatmap of marker expression by the clusters identified (n=38). (C) Immune-cell types in the immune_high and immune_low group are visualised by contour tSNE map. (D) Boxplots (median±SD) depict comparison of indicated cell clusters between immune_high and immune_low group. (E) Spearman correlation matrix of phenograph clusters and clinical parameters. Statistics: Mann-Whitney U test with p values indicated in boxplots, and spearman-correlation (*p<0.05, **p<0.01, ***p<0.001). ALT, alanine-aminotransferase; AST, aspartate-aminotransferase; LDH, lactate dehydrogenase; tSNE, t-distributed stochastic neighbor embedding.

a few naïve T-cells, that were absent in control peripheral blood mononuclear cells (PBMC) (figure 2B–D). High-dimensional phenotypic analysis also showed clearly distinct CD8$^+$T-cell activation and differentiation in the patient's peripheral blood and liver, with high expression of activation and exhaustion markers (CD38, PD-1) and the presence of CD103$^+$CD69$^+$CXCR6$^+$ TRM cells in the inflamed liver (figure 2C,D). Together, these data inform of a significant

Gut: first published as 10.1136/gutjnl-2024-333880 on 5 April 2025. Downloaded from http://gut.bmj.com/ on August 18, 2025 at Koc Universitesi. Protected by copyright, including for uses related to text and data mining, AI training, and similar technologies.

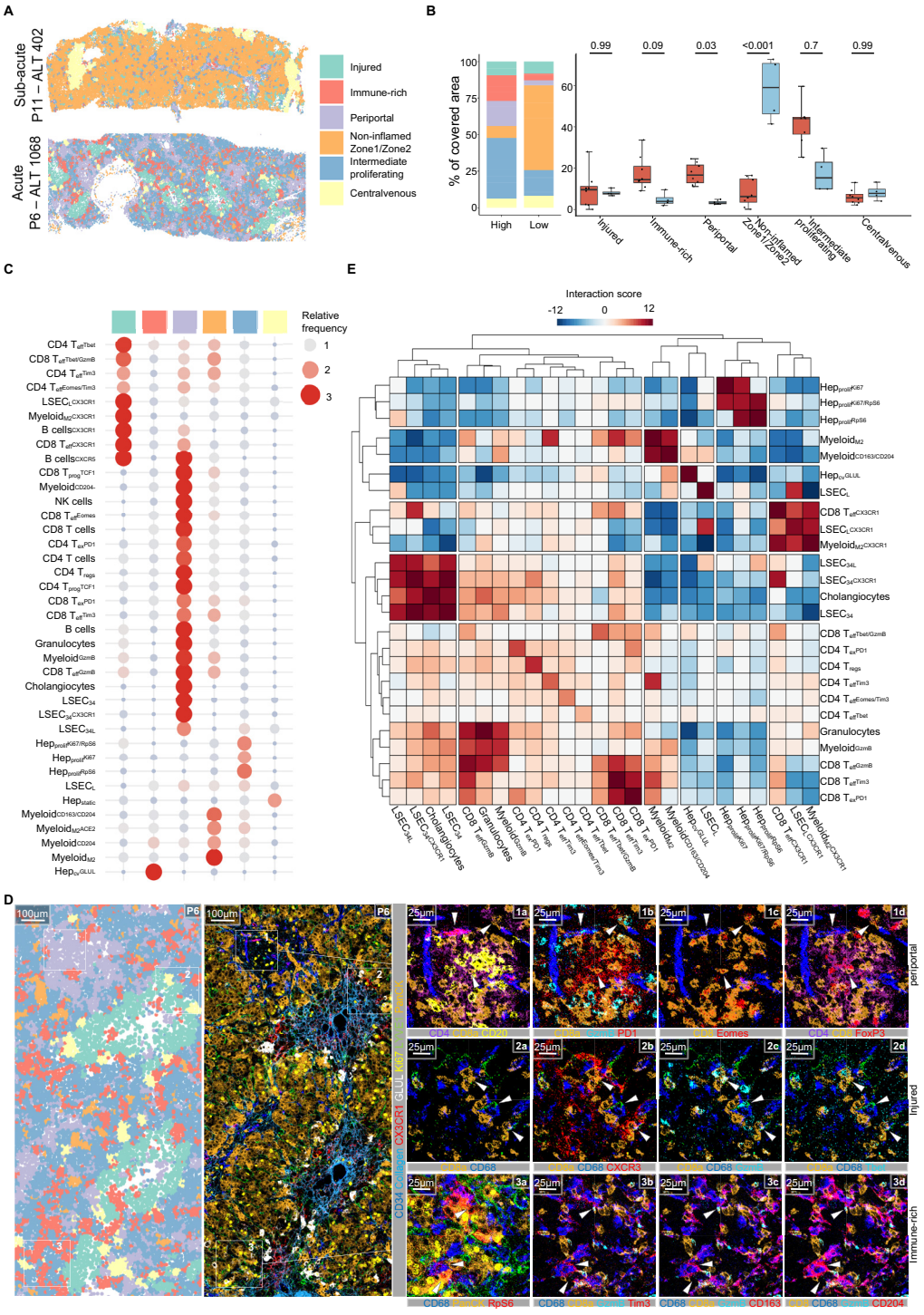


Figure 4 Spatial neighbourhood analysis reveals pathognomonic microanatomic niches and characteristic immune cell interactions. (A) Cellular microenvironments based on centroid-kNN neighbourhoods are visualised on the biopsy tissue from patients P11 and P6. Different neighbourhoods are colourised as indicated in the figure. (B) Neighbourhoods are compared between immune_high versus immune_low groups. Percentage of covered area is depicted by stacked bar chart and box plots. (C) Region map indicates relative cellular cluster frequencies present in neighbourhoods indicated by colour label. (D) Cellular neighbourhoods are visualised on P6 biopsy. (Left) Neighbourhoods visualisation. (Middle) visualisation of individual marker expression. Boxes indicate ROIs. (Right) high-resolution visualisation of ROI1-ROI3. Expression is indicated by colourised marker name on the black bar (CD34 (blue), collagen (lightblue), CXCR3 (red), PanCK (orange), GLUL (white), Ki67 (yellow), Lyve1 (green)) or in ROIs, arrows indicate cells of interest. ROI1 (Periportal): CD4 (purple), CD8a (orange), CD20 (yellow), CD34 (blue), granzyme B (cyan) and PD1/Eomes/FoxP3 (red). Arrows indicate LSEC34CX3CR1, CD8+ TexPD1 and CD8+ TeffGzmB cells. ROI2 (Injured): CD8a (orange), CD68 (blue), CX3CR1 (red), Lyve1 (green), GzmB/Tbet (cyan). Arrows indicate CD8+ TeffCX3CR1, CD8+ TeffTbet/GzmB, LSECL cells. ROI3 (Immune rich): (ROI3a) CD68 (blue), Ki67 (yellow), Lyve1 (green), RpS6 (red), PanCK (orange). (ROI3b-d) CD8a (orange), CD68 (blue), granzyme B (cyan), CD163/CD204/Tim3 (red). (ROI3a-d) Arrows indicate HepprolifKi67/RpS6, CD68+CD163+/CD204+/Tim3+ M2-Myeloids, CD8+ TeffGzmB E Heatmap of cell–cell interactions between clusters, summarised across patients in interaction score (−12 to 12). Significant avoidances are depicted in blue and interactions in red. Statistics: (A) Kruskall-Wallis with Dunn's multiple comparison test (E) testInteractions (imcRtools). P values indicated in boxplots. kNN, k-nearest-neighbour.

Gut: first published as 10.1136/gutjnl-2024-333880 on 5 April 2025. Downloaded from http://gut.bmj.com/ on August 18, 2025 at Koc Universitesi. Protected by copyright, including for uses related to text and data mining, AI training, and similar technologies.

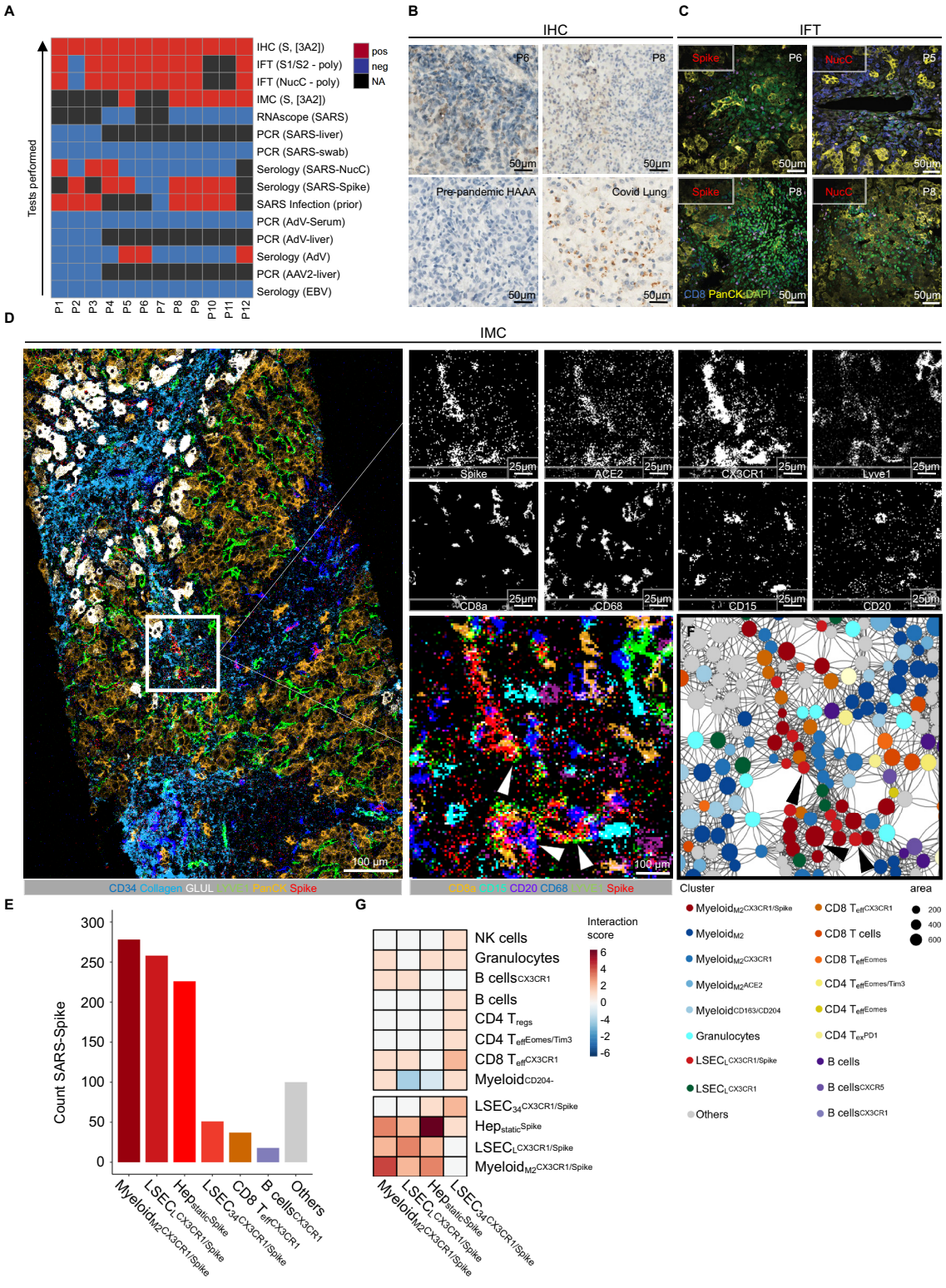


Figure 5 Evidence for COVID-19 antigens in the inflamed hepatic microenvironment associated with the presence of viral receptor ACE2. (A) 14 Covid, AdV, AAV2 and EBV detection tests were performed and summarised per heatmap. Positive results are depicted in red, negative in blue and non-available (NA) tests in black. (B) Exemplary plots of IHC (Spike (3A2)) of P6 and P8, positive lung, historic prepandemic HAAA. (C) Exemplary plots of immunofluorescence tests (IFT) with polyclonal Spike1/2 (S1/S2) or nucleocapsid (NucC) as indicated in P5, P6 and P8. (D) (Left) Visualisation of COVID-19-associated IMC staining. Colourisation of markers is indicated at the bottom. (Top right) Individual expression of Spike, ACE2, CX3CR1, Lyve1, CD8a, CD68, CD15 and CD20 in the indicated ROI are shown by white colouring. (Middle/bottom) Visualisation of CD8a (orange), CD15 (cyan), CD20 (purple), CD68 (blue) and LYVE1 (green), spike (red) coexpression. Arrows indicate spike+ MyeloidM2CX3CR1/Spike and LSECLCX3CR1/Spike cells. (E) Barchart quantification of Spike+ (Spike [3A2]) phenograph clusters. (F) kNN-interaction-nodes depicting Spike+ phenograph clusters and their direction interaction partners in the ROI indicated in (D). (G) Heatmap of statistically significant kNN-interaction-pairs depicted in (F). Scale bars are indicated in the figure. AAV2, adeno-associated virus 2; AdV, adenovirus; EBV, Epstein-Barr virus; HAAA, hepatitis-associated aplastic anaemia; IMC, imaging mass cytometry; kNN, k-nearest-neighbour.

Gut: first published as 10.1136/gutjnl-2024-333880 on 5 April 2025. Downloaded from http://gut.bmj.com/ on August 18, 2025 at Koc Universitesi. Protected by copyright, including for uses related to text and data mining, AI training, and similar technologies.

activation of the T-cell compartment in AHUO patients. Moreover, in a patient from the immune_high group, this intrahepatic activation was mirrored by strong peripheral immune activation.

High-dimensional spatial single-cell analysis identifies cellular correlates of hepatic pathology that differ between severe and mild cases of paediatric AHUO

To understand the detailed cellular composition and immune contexture, we leveraged the high-dimensional spatial data for multilevel cell clustering to more precisely identify immune cell subsets using Phenograph algorithm (figure 3A), identifying 38 distinct parenchymal and immune cell clusters (figure 3B). This analysis revealed additional heterogeneity in the hepatocyte and endothelial cell compartment and identified different subtypes of $CD4^+$ and $CD8^+$T-cells, myeloid cells and B cells as well as granulocytes and NK cells (figure 3B). Several, but not all immune cell subsets were enriched in the immune_high group (figure 3C). Specifically, $CD8^+$T-cell subsets with an activated (Tim-3^+, PD-1^+) or effector-like (Granzyme B^+, $CX3CR1^+$) phenotype were enriched in the immune_high group, together with $CD163^+CD204^+$Tim-3^+ M2-like myeloid cells, as well as a myeloid cell cluster characterised by spatially close interaction with cytotoxic T-cells (myeloid GzmB) (figure 3D). Interestingly, hepatocyte subtypes differed strongly between the immune_high and ommune_low groups. Hepatocytes with differential expression of Ki-67 or mtor target pS6 indicating an active cell cycle typical for proliferating hepatocytes ($Hep_{prolif}^{Ki67/RpS6}$, Hep_{prolif}^{Ki67}, Hep_{prolif}^{RpS6}) were significantly enriched in the immune_high group, while non-proliferative GLUL-negative hepatocytes were enriched in the immune_low group. These cell types, together with NK cells and granulocytes, also displayed a significant correlation with clinical laboratory parameters as measured by bilirubin and ALT/AST levels (figure 3E). In contrast to hepatocytes, we did not observe differences in cholangiocytes or LSEC subtypes (figure 3E). However, a population of Lyve-1^+ LSEC that expressed CX3CR1 was significantly associated with GGT measurements (figure 3D,E). Only myeloid and $CD8^+$T-cell clusters correlated with the histologic ISHAK score (figure 3E). These findings fit a possible regenerative response of hepatocytes to immune-mediated tissue injury in severely inflamed patients with a prominent involvement of activated effector $CD8^+$T-cells and M2-like myeloid cells.

Disease-associated microanatomic cell interactions in injured areas

Immunopathology typically results from interactions between specific immune cell types and respective target cells. We, therefore, asked if the spatial cellular interactions could inform about cells involved in liver pathology. To identify disease-associated spatial interactions, we performed a k-Nearest-Neighbour (kNN)- cellular neighbourhood analysis, which identified six microanatomic hepatic compartments (figure 4A). Spatial and cellular composition analysis revealed that several of these compartments reflected known hepatic zonation (figure 4A–D) as illustrated for the periportal area in figure 4D, region of interest 1 (ROI1) However, there were also immune-rich compartments dominated by myeloid cells (ROI3) as well as a compartment connected to areas of tissue injury with collagen deposition (ROI2). Of note, the cellular composition in the injured areas was dominated by several $CD8^+$ and $CD4^+$T-cell subsets, B cells and CX3CR1 expressing immune cells as well as Lyve-$1^+CX3CR1^+$LSECs (figure 4C). Interestingly, the injured compartment was found similarly in both immune_high and immune_low groups. This compartment differed from a heavily immune-infiltrated periportal compartment that was highly over-represented in patients of the immune_high group (figure 4B). In contrast to the injured compartment, the enrichment of immune cells in the periportal areas in the immune_high group consisted of more diverse adaptive and innate immune cell subtypes (figure 4C). Cellular interaction analysis further identified a distinct interaction pattern between $CX3CR1^+CD8^+$T-cells, LSEC and M2-like myeloid cells (figure 4E), associated with the 'injured' microanatomic compartment (figure 4C,D (ROI2)). These analyses point to a specific role of a pathogenic cellular triad consisting of a $CD8^+$T-cell subset interacting with myeloid and LSEC cells in injured hepatic areas.

Immune correlates of patients with relapse hepatitis

Two patients from the immune_high group (P3, P8) experienced relapse hepatitis after steroid withdrawal. We thus tested for potential differences between the relapse patients in comparison to other patients from the immune_high group (with similar degrees of hepatitis). P8 had the highest density of plasma cells in our dataset (but reduced compared with the classical AIH control group), while no plasma cells were detected in the other relapse patients (P3) (online supplemental figures 2 and 3). Both patients had a relatively high amount of $PD1^+$T-cells at the expense of $TCF1^+$T-cells and a higher amount of $CX3CR1^+$ LSEC cells, together with overall small changes in cellular interactions. These data inform about subtle differences in the observed immune infiltrate in patients with subsequent relapse compared with other immune_high patients.

Detection of intrahepatic SARS-CoV-2 antigens in the patient cohort

We next tested for evidence of different viral infections in our patient cohort using a total of 14 different tests (figure 5A). All patients were tested for adenoviral infection by PCR (serum) and serology. All patients were PCR negative, three patients were positive for adenoviral serology interpreted as reflecting a prior infection (IgG positive). Three patients were further tested for adenoviral PCR and AAV2 specifically in liver tissue (all negative). Since AAV2 infection would require an adenoviral infection as a helper virus, we, therefore, excluded an active AAV2 infection in these cases. For SARS-CoV-2, all patients were negative for PCR (swab) at the time of liver biopsy, however, a substantial fraction of patients reported a recent infection or had serological evidence of prior SARS-CoV-2 infection (figure 5A, table 1). Of note, SARS-CoV-2 proteins can be detected in children's stool significantly longer than a positive PCR can be detected by swab.[31] We, therefore, tested for viral antigens in the liver. As shown in figure 5B, immunoreactivity for Spike antigen was detected across liver samples in the patient cohort but not in a historic HAAA patient. Furthermore, immunofluorescence analysis using different antibodies targeting SARS-CoV-2 spike and nucleocapsid antigens was positive in 11/12 patients tested (figure 5A,C). We asked if these findings reflect active intrahepatic SARS-CoV-2 replication in the liver. SARS-CoV-2 PCR was performed on residual archived formalin-fixed and paraffin-embedded tissue in three patients, but tests were negative. Similarly, RNA-Scope analysis for viral RNA was negative in a further six patients tested (figure 5A). IMC analysis for SARS-CoV-2 antigens

Gut: first published as 10.1136/gutjnl-2024-333880 on 5 April 2025. Downloaded from http://gut.bmj.com/ on August 18, 2025 at Koc Universitesi. Protected by copyright, including for uses related to text and data mining, AI training, and similar technologies.

was possible in 6 AHUO patients and positive in all patients tested. These samples were used to further interrogate the relationship between viral antigen, its receptor ACE2 and the involved cell types.

SARS-CoV-2 antigens are detected in association with ACE2 expression in LSECs, myeloid cells and hepatocytes

We first inspected areas with positive SARS-CoV-2 Spike expression in LSEC cells and found that Spike signal was often co-localised with cells expressing the receptor ACE2 (figure 5D). LSECs, M2-like myeloid cells and hepatocytes represented the majority of cells staining positive for Spike (figure 5E).

Spike protein aggregates were found to colocalise with ACE2 expression in hepatocyte-depleted and collagen-rich 'injured' regions with abundant CX3CR1$^+$ cells (figure 5D). Spike$^+$ ACE2 expressing $LSEC_{34}^{CX3CR1}$ and $LSEC_{L}^{CX3CR1}$ as well as $Myeloid_{M2}^{CX3CR1}$ showed significant interactions with CX3CR1 effector-like CD8+T cells, B cells and granulocytes (figure 5E,F), as expected from our interaction analysis performed in the complete cohort (figure 4). In addition, Tim-3 expressing CD4 T-cells and Tregs interacted with $LSEC_{34}^{CX3CR1}$. We next performed an interaction analysis of spike$^+$ cells. Hepatocytes positive for spike protein interacted significantly with granulocytes (figure 5G). Strong interactions were also observed between Spike-positive myeloid and $LSEC_L$ cells, and these cells were additionally interacting with CD8 effector T-cells expressing CX3CR1 (figure 5G), reflecting the pathogenic cellular triad identified in our prior analysis. Together, the single-cell expression and spatial interaction analyses suggest an immune response involving CD8$^+$T effector cells, myeloid cells and granulocytes targeting hepatocytes and LSEC cells that stain positive for Spike antigens. These interactions could drive postacute COVID-19-related immunity involved in acute hepatitis.

DISCUSSION

The rise of severe cases of AHUO coinciding with the reduction of hygiene regulations due to the pandemic in the UK in 2022 was subsequently linked to a rise in cases of adenoviral infection.[11] Here, through the analysis of paediatric AHUO liver samples from a comparable time period in a European cohort, we have identified immune-mediated injury associated with the detection of SARS-CoV-2 antigens, pointing to a possible association with prior SARS-CoV-2 infection, suggesting that the hepatic disease could have manifested as a PASC.

Virological testing of patients presenting with NAEH and fulfilling the WHO AHUO criteria included a thorough workup of hepatological differential diagnoses. Adenoviral infection was assessed using PCR and serology methods. PCR was negative in all patients, one patient had detectable adenoviral IgM/IgG, and two patients had detectable adenoviral IgG. In contrast, 10/12 patients had a history or serologic evidence of SARS-CoV-2 infection. Histological analysis of liver samples for the presence of SARS-CoV-2 Spike or nucleocapsid antigens using IHC, IF and IMC methods resulted in the detection of viral protein in 11/12 patients. Using highly multiplexed IMC analysis, we found significant immune infiltration, in particular, the degree of CD8$^+$T-cell infiltration was linked to the degree of hepatic damage. Our findings are consistent with previous studies that performed immunophenotyping in NAEH/indeterminate PALF and highlighted the dominance of CD8$^+$, CD103$^+$ and Perforin$^+$ T-cell infiltrates.[21 32] We further expand the current understanding by providing an in-depth immunocharacterisation that allowed us to identify distinct microanatomic interaction patterns of T-cell subsets with LSEC and myeloid cells in areas of hepatic injury. Their location and association with the highest clinical severity suggest a pathogenic role as drivers of disease.

However, we also note evidence of wound-healing programmes in the severely inflamed liver. For example, we observe proliferating hepatocytes adjacent to injured areas suggesting indicating a tissue regenerative response mediated by responding hepatocytes. Notably, we also observed that LSECs undergo adaptations as Lyve1/CD34 positive LSEC indicating reactive capillarisation were increasingly found in these areas and interacted with the proliferating hepatocytes, as illustrated in figure 4. These findings fit the recent description of the liver regenerative response in models of acute hepatitis by Matchett *et al* in which migratory hepatocytes with similar localisation at the edge of injury initiate wound closure and regeneration.[33]

Moreover, we highlighted an association between the severity of the clinical course and the degree of intrahepatic T-cell infiltration which was mirrored by strong immune activation in peripheral blood. This could be of diagnostic importance when obtaining a liver biopsy might not be feasible and such a peripheral blood-based immunoprofiling approach was recently successfully applied in a North American cohort of PALF cases.[34]

Notably, hepatic spike antigen was detected in LSECs and myeloid cells that express viral co-receptor ACE2. These cells represent classical antigen-presenting cells of the liver and have immune gatekeeping functions. In the patient cohorts, they were frequently neighboured by cytotoxic CD8$^+$T-cells, suggesting a possible antigen-mediated immune pathology. In our cohort, SARS-CoV-2 PCR analysis of intrahepatic samples was possible on archived material from three patients and a further six patients could be analysed by RNAScope, however, no active hepatic infection could be detected. While a reduced sensitivity of our assay on the archived material cannot be excluded, these results would also be compatible with a model in which a reservoir of SARS-CoV-2 virus exists outside of the liver, but viral antigens can bind to cells expressing the viral receptor and trigger a severe immunopathology.

A possible candidate for the viral reservoir in children is the gastrointestinal tract. Increased epithelial barrier permeability could contribute to enhanced accumulation of SARS-CoV-2 proteins or microbial products into the portal vein and subsequently the liver, where they could trigger inflammation. This mechanism is also discussed for children with COVID-19-related multisystem inflammatory syndrome (MIS-C) that had detectable SARS-CoV-2 RNA in stool weeks after initial infection when nasal swabs were long negative.[31 35] In another work, the authors also found SARS-CoV-2 spike protein in plasma together with biomarkers (zonulin) for disturbed intestinal barrier function.[35] It is possible that similar mechanisms could drive the SARS-CoV-2-related AHUO here. While no material was available for these analyses in our cohort, stool samples should be investigated for presence of SARS-CoV-2 in subsequent patients.

Further similarities to MIS-C exist. In MIS-C children, enrichment of CX3CR1$^+$ CD8$^+$ T-cells associated with vascular pathology was identified.[36] Patients included in our cohort did not fit the criteria for MIS-C, but we could also observe a prominent infiltration of CX3CR1$^+$ CD8$^+$ T-cells in the injured liver in our patients. Another similarity is the delayed onset of liver inflammation after a putative COVID-19 infection in our cohort, which is typical in MIS-C patients. Thus, it remains a possibility that similar underlying immune mechanisms could be prevalent in MIS-C and drive postacute COVID-19-associated hepatitis.

Overall, the pathomechanisms driving AHUO in our cohort seem to differ from the outbreak in the UK. In that cohort, AAV2 in plasma and liver samples was detected in 81% (26/31) patients and linked

Gut: first published as 10.1136/gutjnl-2024-333880 on 5 April 2025. Downloaded from http://gut.bmj.com/ on August 18, 2025 at Koc Universitesi. Protected by copyright, including for uses related to text and data mining, AI training, and similar technologies.

to CD4+ T-cell mediated pathology.[9] Interestingly, even in these cohorts, SARS-CoV-2 PCR was positive in 8.9%–12.8% of cases[5 8] and 52% of patients tested positive for SARS-CoV-2-nucleocapsid IgG.[9] These data likely indicate that in the UK cohort, AAV2 infection—whether independent or in conjunction with SARS-CoV-2—represented the major risk factor for driving the epidemic rise of AHUO cases. Nevertheless, a similar rise in AAV2 cases was not observed in most central European cohorts.[15] Our data suggest that COVID-19 can drive AHUO as a PASC manifestation independent of AAV2. It is in line with a report of five paediatric cases of NAEH, two requiring LT, that were associated with prior COVID-19 infection.[3] Moreover, a Dutch case series in NAEH reported three of five patients with prior COVID-19 infection.[37] In sum, in cases of paediatric AHUO patients, prior COVID-19 infection needs to be considered independent of adenoviral infection. These results have clinical implications. For example, antiviral therapy with cidofovir has been used as an antiadenoviral therapeutic option.[14] The use of immunosuppressive therapy was considered rational given the significant amount of immune infiltration observed in our analysis, as well as the utility in other cases of NAEH and HAAA.[22] In our cohort, 10/12 patients received early steroid therapy and no patient progressed to require LT.

Our work has limitations. Due to the low amount of tissue material available in this paediatric patient cohort, not all methods could be applied to all samples. A precise retrospective determination of the exact date of prior COVID-19 infection was often not possible. In patients receiving comedication, an additional contribution of drug-associated liver injury (DILI) mechanisms may have contributed to liver pathology. Indeed, histopathological assessment by a blinded hepatopathologist indicated that several patients had histological features compatible with additional DILI, such as eosinophilic infiltration. However, DILI in children is rare and, in our cohort, these DILI features were not found dominant. Moreover, our spatial immunophenotyping and virological data suggest that potential DILI did not strongly modify the PASC-related immune response in these patients. Our work also suggests that the use of steroids is effective in this patient cohort; however, this should be further tested in a prospective trial. Steroid use could explain why surveillance metrics in transplant networks did not detect a strong COVID-19-associated rise in paediatric patients requiring liver transplants.

In sum, our work identifies immune-mediated acute hepatitis in children as a possible PASC and associated with a characteristic immune infiltrate. Paediatric patients with AHUO should be assessed for a history of COVID-19 infection and may respond to immunosuppressive therapy.

MATERIAL AND METHODS

Sex as a biological variable

Patients were recruited independent of sex. 8/12 patients were female and 4/12 were male. We observed no sex-associated significant differences for age, ALT, AST, bilirubin, LDH, INR or ISHAK score or clinical symptoms. GGt (U/L) levels were increased sevenfold in females (median f/m: 264.5/37.5 U/L, Mann-Whitney: $p<0.01$).

Patient inclusion

Patient inclusion was based on severe hepatitis >10×ULN (grade 3 according to CTCAE V.5.0) and applying the WHO criteria for acute hepatitis of unknown aetiology: a person presenting with an acute hepatitis (non-hep A–E) with serum transaminase >500 IU/L (AST or ALT), who is 16 years and younger, since 1 October 2021.[38] Pre-existing liver disease, acute toxic or viral A–E hepatitis were ruled out by careful history, and biochemical and viral investigations. 13 patients were recruited into the study, 1 patient was subsequently excluded due to diagnosis of Wilson's disease.

To compare immune cell infiltration and detection of viral proteins, different biobanked control samples were investigated: a historic prepandemic, age-matched liver biopsy from an AHUO patient subsequently diagnosed with HAAA, five macroscopically healthy liver tissues obtained during surgery for colorectal cancer metastasis in distant liver tissues, five liver biopsies from patients with classical AIH, positive lung control samples for SARS-CoV-2 as described in,[25] as well as PBMC from a healthy donor.

Patient and public involvement

Patients contributed biomaterials but they or the public were not involved in the design, or conduct, or reporting of our research. Dissemination plans include press releases targeted to post-COVID-19 patient networks.

Statistics

Statistical analysis was performed using GraphPad prism V.10. In boxplots, individual data points are indicated as dots, their median value and the p values of indicated comparison are depicted in the referring boxes. Non-parametric distribution was assumed.

Mann-Whitney test was performed in figures 1D, F, 2A, 3B. Kruskall-Wallis with Dunn's multiple comparison test was performed in figures 1D, 4B, when comparing immune_high versus immune_low versus controls. A paired-Wilcoxon test was performed in figure 2A comparing paired liver-PBMC samples. Spearman correlation was performed using R studio (corrplot) in figures 1E, 2D. Cell–cell interactions were analysed in figures 4D, 5E. Briefly, the testInteraction function in imcRtools (method='classic) following the kNN-interaction-graph with the same settings was used.[39] In figures 1E, 2D, p values are indicated by asterisks: *p>0.05, **p>0.01, ***p>0.001.

Author affiliations
[1]Clinic for Internal Medicine II, Freiburg University Medical Center, Freiburg im Breisgau, Germany
[2]Division of Internal Medicine I, Gastroenterology, Hepatology Endocrinology & Metabolism, Medical University Innsbruck, Innsbruck, Austria
[3]Institute of Pathology, School of Medicine and Health, Technical University of Munich, München, Germany
[4]Koc University School of Medicine, Pediatric GI and Hepatology Liver Transplantation Center, Koc Universitesi, Istanbul, Turkey
[5]Center for Virology, Medical University of Vienna, Wien, Austria
[6]Department of Pediatrics and Adolescent Medicine, St. Anna Children's Hospital, Medical University Vienna, Vienna, Austria
[7]Department of Pediatrics and Adolescent Medicine, Division of Pediatric Pulmonology, Allergology and Endocrinology, Medical University of Vienna, Vienna, Austria
[8]Department of Pediatric Gastroenterology, Dr. von Hauner Children's Hospital, University Hospital Munich, Munich, Germany
[9]Department of Pediatric and Adolescent Medicine, University Medical Center Ulm, Ulm, Germany
[10]Department of Pediatric and Adolescent Medicine, Josefinum Hospital, Augsburg, Germany
[11]Department of Pediatrics, Centro Hospitalar e Universitário de Coimbra, Coimbra, Portugal
[12]Institute of Virology, Freiburg University Medical Center, Freiburg im Breisgau, Germany
[13]Department of Paediatrics I, Medical University of Innsbruck, Innsbruck, Austria
[14]Institute of Cell Biology, Biocenter, Medical University of Innsbruck, Innsbruck, Austria

Gut: first published as 10.1136/gutjnl-2024-333880 on 5 April 2025. Downloaded from http://gut.bmj.com/ on August 18, 2025 at Koc Universitesi. Protected by copyright, including for uses related to text and data mining, AI training, and similar technologies.

[15]German Cancer Consortium (DKTK) Heidelberg, Germany, Partner Site Freiburg, Freiburg, Germany

Acknowledgements We thank all patients and parents who participated in this study. We thank Patricia Otto-Mora and Dr. Jürgen Beck for excellent assistance with imaging mass cytometry.

Contributors Samples and clinical data were collected by TM, GFV, AZ, CA, SN, IG, HK, AV, EL, FIM and LW. Histological stainings (HE, IMC, IHC and IFT) were performed by LKrimmel, AZ and FR. CM performed pathology analysis and quantified histological features. Spatial IMC analysis was performed by FR. FACS stainings and analysis were performed by VK, AG and MY. Adenovirus-PCR was performed by JHA and SWA. RNAscope was performed by LKern and MS. GFV and BB designed and supervised the study. BB, GFV and FR wrote the manuscript. TM, TB, PH, RT and MH proofread the manuscript and revised it for important intellectual content. BB is the guarantor. ChatGPT was used for generating Rstudio code and debugging of figures and analysis.

Funding The research was supported by grants from the Deutsche Forschungsgemeinschaft (DFG) # 520992132 to BB, # 441891347 (OncoEscape), # 390939984 (CIBSS), # 272983813 (TRR179), # 256073931 (IMPATH) and # 518316185 (GMCA) and the Deutsche Forschungsgemeinschaft (DFG, German Research Foundation)—Project-ID 272983813—TRR 179 to CM.

Competing interests BB is a patent holder on methods and compositions for treating diseases associated with exhausted T-cells.

Patient and public involvement Patients and/or the public were not involved in the design, or conduct, or reporting, or dissemination plans of this research.

Patient consent for publication Not applicable.

Ethics approval This study involves human participants and this study was conducted conforming to the guidelines of the Institutional Review Board of the Medical University of Innsbruck (Ethics vote #1029/2017), University of Freiburg (Ethics vote #322/20), the 2013 Declaration of Helsinki and the 2018 Declaration of Istanbul. Written consent was given in writing by all individuals and legal guardians. Participants gave informed consent to participate in the study before taking part.

Provenance and peer review Not commissioned; externally peer reviewed.

Data availability statement Data are available in a public, open access repository. The imaging data and high-resolution versions of the figures illustrating IMC data are available at zenondo.org (reference: 40) 10.5281/zenodo.14097945. The clinical data isare listed in tables in this manuscript.

Supplemental material This content has been supplied by the author(s). It has not been vetted by BMJ Publishing Group Limited (BMJ) and may not have been peer-reviewed. Any opinions or recommendations discussed are solely those of the author(s) and are not endorsed by BMJ. BMJ disclaims all liability and responsibility arising from any reliance placed on the content. Where the content includes any translated material, BMJ does not warrant the accuracy and reliability of the translations (including but not limited to local regulations, clinical guidelines, terminology, drug names and drug dosages), and is not responsible for any error and/or omissions arising from translation and adaptation or otherwise.

Open access This is an open access article distributed in accordance with the Creative Commons Attribution Non Commercial (CC BY-NC 4.0) license, which permits others to distribute, remix, adapt, build upon this work non-commercially, and license their derivative works on different terms, provided the original work is properly cited, appropriate credit is given, any changes made indicated, and the use is non-commercial. See: http://creativecommons.org/licenses/by-nc/4.0/.

ORCID iDs
Andreas Zollner http://orcid.org/0000-0001-6095-068X
Henrike Salié http://orcid.org/0000-0002-2993-3782
Laurenz Krimmel http://orcid.org/0000-0002-8811-9289
Tobias Boettler http://orcid.org/0000-0002-1195-055X
Maike Hofmann http://orcid.org/0000-0001-8410-8833
Peter Hasselblatt http://orcid.org/0000-0002-1107-6516
Robert Thimme http://orcid.org/0000-0003-1417-4135
Herbert Tilg http://orcid.org/0000-0002-4235-2579
Thomas Müller http://orcid.org/0000-0001-8908-5589
Georg Friedrich Vogel http://orcid.org/0000-0002-2515-4490
Bertram Bengsch http://orcid.org/0000-0003-2552-740X

REFERENCES

1 Baker JM, Buchfellner M, Britt W, *et al*. Acute Hepatitis and Adenovirus Infection Among Children - Alabama, October 2021-February 2022. *MMWR Morb Mortal Wkly Rep* 2022;71:638–40.
2 The Lancet Infectious Diseases. Explaining the unexplained hepatitis in children. *Lancet Infect Dis* 2022;22:743.
3 Cooper S, Tobar A, Konen O, *et al*. Long COVID-19 Liver Manifestation in Children. *J Pediatr Gastroenterol Nutr* 2022;75:244–51.
4 Marsh K, Tayler R, Pollock L, *et al*. Investigation into cases of hepatitis of unknown aetiology among young children, Scotland, 1 January 2022 to 12 April 2022. *Euro Surveill* 2022;27:2200318.
5 Bengsch B, Ohtani T, Khan O, *et al*. Epigenomic-Guided Mass Cytometry Profiling Reveals Disease-Specific Features of Exhausted CD8 T Cells. *Immunity* 2018;48:1029–45.
6 Chronister WD, Crinklaw A, Mahajan S, *et al*. TCRMatch: Predicting T-Cell Receptor Specificity Based on Sequence Similarity to Previously Characterized Receptors. *Front Immunol* 2021;12:640725.
7 Kelgeri C, Couper M, Gupte GL, *et al*. Clinical Spectrum of Children with Acute Hepatitis of Unknown Cause. *N Engl J Med* 2022;387:611–9.
8 Romaní Vidal A, Vaughan A, Innocenti F, *et al*. Hepatitis of unknown aetiology in children - epidemiological overview of cases reported in Europe, 1 January to 16 June 2022. *Euro Surveill* 2022;27:2200483.
9 Jagadisan B, Verma A, Deheragoda M, *et al*. Outbreak of indeterminate acute liver failure in children with adenoviraemia - Not a new disease. *J Hepatol* 2023;79:43–9.
10 Morfopoulou S, Buddle S, Torres Montaguth OE, *et al*. Genomic investigations of unexplained acute hepatitis in children. *Nature New Biol* 2023;617:564–73.
11 Ho A, Orton R, Tayler R, *et al*. Adeno-associated virus 2 infection in children with non-A-E hepatitis. *Nature New Biol* 2023;617:555–63.
12 Mitchell MM, Leng Y, Boppana S, *et al*. Signatures of AAV-2 immunity are enriched in children with severe acute hepatitis of unknown etiology. *Sci Transl Med* 2023;15:eadh9917.
13 Servellita V, Sotomayor Gonzalez A, Lamson DM, *et al*. Adeno-associated virus type 2 in US children with acute severe hepatitis. *Nature New Biol* 2023;617:574–80.
14 Verma A, Vimalesvaran S, Lampejo T, *et al*. Use of cidofovir in recent outbreak of adenovirus-associated acute liver failure in children. *Lancet Gastroenterol Hepatol* 2022;7:700–2.
15 Leiskau C, Tsaka S, Meyer-Ruhnke L, *et al*. Acute severe non-A-E-hepatitis of unknown origin in children - A 30-year retrospective observational study from north-west Germany. *J Hepatol* 2023;78:971–8.
16 Chapin CA, Diamond T, Harris RM, *et al*. Adenovirus is Not Detected in Liver Tissue From a Historical Multicenter Cohort of Children With Acute Liver Failure. *J Pediatr Gastroenterol Nutr* 2023;77:393–5.
17 European Centre for Disease Prevention andControl/WHO Regional Office for Europe. Hepatitis of unknown aetiologyin children, joint epidemiological overview. 2022. Available: https://cdn.ecdc.europa.eu/novhep-surveillance/
18 Kemme S, Stahl M, Brigham D, *et al*. Outcomes of Severe Seronegative Hepatitis-associated Aplastic Anemia: A Pediatric Case Series. *J Pediatr Gastroenterol Nutr* 2021;72:194–201.
19 Tüfekçi Ö, Özdemir HH, Malbora B, *et al*. Hepatitis-Associated Aplastic Anemia: Etiology, Clinical Characteristics and Outcome. *J Pediatr Hematol Oncol* 2022;44:e223–6.
20 Wanner N, Andrieux G, Badia-I-Mompel P, *et al*. Molecular consequences of SARS-CoV-2 liver tropism. *Nat Metab* 2022;4:310–9.
21 Chapin CA, Melin-Aldana H, Kreiger PA, *et al*. Activated CD8 T-cell Hepatitis in Children With Indeterminate Acute Liver Failure: Results From a Multicenter Cohort. *J Pediatr Gastroenterol Nutr* 2020;71:713–9.
22 Chapin CA, Horslen SP, Squires JE, *et al*. Corticosteroid Therapy for Indeterminate Pediatric Acute Liver Failure and Aplastic Anemia with Acute Hepatitis. *J Pediatr* 2019;208:23–9.
23 Nishiura H, Jung SM, Hayashi K. High population burden of Omicron variant (B.1.1.529) is associated with the emergence of severe hepatitis of unknown etiology in children. *Int J Infect Dis* 2022;122:30–2.
24 Marjot T, Webb GJ, Barritt AS 4th, *et al*. COVID-19 and liver disease: mechanistic and clinical perspectives. *Nat Rev Gastroenterol Hepatol* 2021;18:348–64.
25 Schwabenland M, Salié H, Tanevski J, *et al*. Deep spatial profiling of human COVID-19 brains reveals neuroinflammation with distinct microanatomical microglia-T-cell interactions. *Immunity* 2021;54:1594–610.
26 Boettler T, Csernalabics B, Salié H, *et al*. SARS-CoV-2 vaccination can elicit a CD8 T-cell dominant hepatitis. *J Hepatol* 2022;77:653–9.
27 Uzun S, Zinner CP, Beenen AC, *et al*. Morphologic and molecular analysis of liver injury after SARS-CoV-2 vaccination reveals distinct characteristics. *J Hepatol* 2023;79:666–76.
28 Bowe B, Xie Y, Al-Aly Z. Postacute sequelae of COVID-19 at 2 years. *Nat Med* 2023;29:2347–57.
29 Liang J, Kelly DR, Pai A, *et al*. Clinicopathologic Features of Severe Acute Hepatitis Associated With Adenovirus Infection in Children. *Am J Surg Pathol* 2023;47:977–89.
30 Wührl M, Ringelhan M, Ehmer U, *et al*. (Seltene) infektiöse Hepatitiden als wichtige Differenzialdiagnose der unklaren Hepatopathie. *Pathologie* 2023;44:53–62.
31 Holm-Jacobsen JN, Bundgaard-Nielsen C, Rold LS, *et al*. The Prevalence and Clinical Implications of Rectal SARS-CoV-2 Shedding in Danish COVID-19 Patients and the General Population. *Front Med (Lausanne)* 2021;8:804804.
32 Chapin CA, Burn T, Meijome T, *et al*. Indeterminate pediatric acute liver failure is uniquely characterized by a CD103+CD8+ T-cell infiltrate. *Hepatology* 2018;68:1087–100.
33 Matchett KP, Wilson-Kanamori JR, Portman JR, *et al*. Multimodal decoding of human liver regeneration. *Nature New Biol* 2024;630:158–65.

Gut: first published as 10.1136/gutjnl-2024-333880 on 5 April 2025. Downloaded from http://gut.bmj.com/ on August 18, 2025 at Koc Universitesi. Protected by copyright, including for uses related to text and data mining, AI training, and similar technologies.

34 Chapin CA, Diamond T, Perez A, *et al*. Identification of pediatric activated T-cell hepatitis using clinical immune studies. *Clin Res Hepatol Gastroenterol* 2024;48:102407.
35 Yonker LM, Gilboa T, Ogata AF, *et al*. Multisystem inflammatory syndrome in children is driven by zonulin-dependent loss of gut mucosal barrier. *J Clin Invest* 2021;131:e149633.
36 Vella LA, Giles JR, Baxter AE, *et al*. Deep immune profiling of MIS-C demonstrates marked but transient immune activation compared to adult and pediatric COVID-19. *Sci Immunol* 2021;6:eabf7570.
37 Lexmond WS, de Meijer VE, Scheenstra R, *et al*. Indeterminate pediatric acute liver failure: Clinical characteristics of a temporal cluster of five children in the Netherlands in the spring of 2022. *United European Gastroenterol J* 2022;10:795–804.
38 World Health Organization. Disease outbreak news; multi-country – acute, severe hepatitis of unknown origin in children. 2022. Available: https://www.who.int/emergencies/disease-outbreak-news/item/2022-DON376
39 Windhager J, Zanotelli VRT, Schulz D, *et al*. An end-to-end workflow for multiplexed image processing and analysis. *Nat Protoc* 2023;18:3565–613.
40 Bengsch B, Roettele F, Vogel G, *et al*. Data from: imaging mass cytometry of pediatric liver biopsies in patients with ahuo and possible pasc. Zenodo, 2024. Available: https://doi.org/10.5281/zenodo.14097945

Gut: first published as 10.1136/gutjnl-2024-333880 on 5 April 2025. Downloaded from http://gut.bmj.com/ on August 18, 2025 at Koc Universitesi. Protected by copyright, including for uses related to text and data mining, AI training, and similar technologies.